To: **Journal of Materials Chemistry A**

Correlation between Electroconductive and Structural Properties of Proton Conductive Acceptor-Doped Barium Zirconate

Donglin Han [a*], Kozo Shinoda [b], Shigeo Sato [c], Masatoshi Majima [d], Tetsuya Uda [a*]

[a] Department of Materials Science and Engineering, Kyoto University,

Yoshida Honmachi, Sakyo-ku, Kyoto 606-8501, Japan

[b] Institute of Multidisciplinary Research for Advanced Materials, Tohoku University,

Katahira 2-1-1, Aoba-ku, Sendai 980-8577, Japan

[c] Graduate School of Science and Engineering, Ibaraki University

4-12-1 Nakanarusawa, Hitachi 316-8511, Japan

[d] Sumitomo Electric Industries, Ltd.,

1-1-1, Koyakita, Itami-shi, Hyogo 664-0016, Japan

* Corresponding author: Donglin Han (han.donglin.8n@kyoto-u.ac.jp)

and Tetsuya Uda (materials_process@aqua.mtl.kyoto-u.ac.jp)

TEL: +81-75-753-5445, FAX: +81-75-753-5284

Abstract

In this work, various dopants were doped into $BaZrO_3$, and the conductivities, proton concentrations, site occupancy of the dopants, and the lattice volume change due to chemical expansion were investigated. The dopants belonging to the lanthanide group occupy both the Ba and Zr-sites, but their amount in the Ba-site is quite limited to influence the conductivity significantly. The samples doped with Yb, Tm Er, Y and Ho exhibit both the high proton concentration and high conductivity, together with relatively large lattice expansion due to hydration. It was thereby suggested that in most cases, the proton concentration, proton conductivity and lattice change due to chemical expansion behaves in a correlated way in the proton conductive acceptor-doped $BaZrO_3$. However, the Sc-doped $BaZrO_3$ seems to be different. Its proton concentration is high, but the conductivity and the lattice change due to chemical expansion effect are relatively small. This factor indicates that the conductivity is strongly related to the lattice expansion due to hydration rather than simply the proton concentration.

Keywords: Barium zirconate, Site occupancy, Chemical expansion, Hydration, Proton conductor

1. Introduction

Proton conductive barium zirconate ($BaZrO_3$), in which tetravalent Zr host cations are partially substituted by trivalent dopants, is receiving increasing interest due to its promising electrochemical application, such as an electrolyte in protonic ceramic fuel cells (PCFCs) [1, 2]. Generally, yttrium (Y) is regarded to be a proper dopant, since by doping 20 mol% Y ($BaZr_{0.8}Y_{0.2}O_{3-\delta}$), proton conductivity higher than 10^{-2} Scm^{-1} generates at 600 °C in a humid environment [3-5]. In addition, some lanthanide dopants, like holmium (Ho) and ytterbium (Yb), also impart high proton conductivity [6, 7]. What is the optimal dopant for the proton conductive $BaZrO_3$ is always a greatly important and highly concerned question [8], but as far as we know, it has not been answered. Although trivalent dopants are intentionally introduced to replace the Zr cations, it happens for them to substitute divalent Ba cations [5, 9-12]. Under such circumstances, oxide ion vacancies ($V_O^{\bullet\bullet}$) are consumed for charge compensation. The Ba-site occupation is therefore detrimental to the incorporation of protons (in the form of hydroxide groups ($OH_O^{\bullet}$)) through a hydration process (eqn (1)) where participation of oxide ion vacancies is necessary [11-15].

$$H_2O + V_O^{\bullet\bullet} + O_O^{\times} \rightarrow 2OH_O^{\bullet} \tag{1}$$

The hydration process also exhibits significant structural influence, such as chemical expansion in lattice volume due to water uptake. [10, 14, 16-19] Since such chemical expansion generates compressional and tensional stresses during hydration and dehydration, respectively, risk of mechanical failure in electrolyte is therefore raised. [20] It is meaningful to mention here that we previously reported a co-existence of two perovskite phases in 20 mol% Y-doped $BaZrO_3$ due to difference in hydration degree. [9] The same sample was kept in a dessicator for two years, and the X-ray diffraction (XRD) pattern was collected again. We found that the intensity of the highly hydrated phase increased significantly (**Fig 1**), indicating that the hydration process would proceed even at room temperature in a controlled atmosphere with low partial pressure of water vapor.

In this work, various dopants were doped into $BaZrO_3$. A systematic investigation on conductivity, water content, site occupancies of the dopants, and chemical expansion due to hydration were performed. The dependence of proton conduction on dopants was thereby determined, and a correlation between these specific behaviors and properties is clarified.

2. Experimental

2.1 Material preparation

Undoped $BaZrO_3$ and the samples containing 20 mol% dopants ($BaZr_{0.8}M_{0.2}O_{3-\delta}$ (BZM20), M = Sc, Y, In, Pr, Nd, Sm, Eu, Gd, Tb, Dy, Ho, Er, Tm and Yb were prepared by a conventional solid state reaction method. Starting materials of $BaCO_3$, ZrO_2, and monoxides containing relevant dopant elements (Sc_2O_3, Y_2O_3, In_2O_3, Pr_6O_{11}, Nd_2O_3, Sm_2O_3, Eu_2O_3, Gd_2O_3, Tb_4O_7, Dy_2O_3, Ho_2O_3, Er_2O_3, Tm_2O_3 and Yb_2O_3) were mixed at the desired ratios, and ball-milled for 24 h. Mixtures were then pressed into pellets under 9.8 MPa and heat-treated at 1000 ^{o}C for 10 h. After ball-milling for 10 h, the samples were pressed into pellets under 9.8 MPa again, and kept at 1300 ^{o}C for 10 h for synthesizing. The samples were ball-milled for 24 h, and subsequently mixed with an organic binder solution consisting of water, polyvinyl alcohol, glycerin, and ethanol. The samples were then pressed into pellets at 392 MPa, and heat-treated at 600 ^{o}C for 8 h to remove the binder solution. At last, after being buried in sacrificial powders which are mixtures of the relevant synthesized BZM20 powders (99 wt%) and $BaCO_3$ (1 wt%), the pellet-like samples were heated at 1600 ^{o}C for 24 h in oxygen atmosphere for sintering, and finally quenched in ambient atmosphere. A photograph of the as-sintered pellet-like samples was given in **Fig. 2**.

2.2 Characterization

Since the 20 mol% Nd-doped sample is not a single perovskite phase [7], only the samples doped with Pr, Gd, Tb, Ho, Er, Tm, Yb and In were proceeded for detailed characterization. Structure of the powder-like samples was examined by X-ray diffraction (XRD) analysis in ambient atmosphere in Bragg-Brentano (θ-2θ) geometry with D8 ADVANCE (Bruker AXS GmbH, Karlsruhe, Germany) equipped with a Cu $K\alpha$ radiation source. Incident X-ray was monochromated to the Cu $K\alpha_1$ (0.15406 nm) with a Johansson-type monochromator of quartz-101 reflection. High temperature XRD (HT-XRD) measurements were performed using Cu $K\alpha$ radiation with X'Pert-ProMPD (PANalytical, Almelo, Netherland), which was equipped with a HTK 1200N high-temperature chamber (Anton Paar, Graz, Austria). Dry or wet ($p_{\mathrm{H_2O}}$ = 0.0312 atm) oxygen gas was flowed in the high-temperature chamber. HT-XRD patterns were collected during cooling from 1000 to 30

^{o}C at an average cooling rate about 1.06 $^{o}Cmin^{-1}$. Detailed procedures of HT-XRD measurements were described in our previous works [17, 18] Rietveld refinement was carried out by utilizing a commercial software TOPAS (Bruker AXS GmbH, Karlsruhe, Germany). Chemical compositions of the samples were determined by inductively coupled plasma atomic emission spectroscopy (ICP-AES) with SPS4000 (Seiko Instruments Inc., Chiba, Japan).

Water contents were determined by Karl-Fischer titration method to give a direct evaluation of proton concentration in the samples. The pellet-like samples heat-treated at 1600 ^{o}C for sintering were broken into pieces about 2 mm in length, and hydrated at 300 ^{o}C in wet O_2 (p_{H_2O} = 0.05 atm) for 7 days. Readers are referred to our previous works [21, 22] for detailed procedures.

All the samples were subjected to conductivity measurements in wet and dry H_2 atmospheres. Water partial pressure in the wet atmosphere was kept at 0.05 atm. Palladium was electrolessly deposited as electrodes. Impedance spectra were collected by A. C. impedance spectroscopy in the frequency range from 10 Hz to 7 MHz using a frequency response analyzer (Solartron SI 1260, Solartron Analytical, UK) with applied voltage of 100 mV at temperature from 600 to 100 ^{o}C.

3. Results

3.1 Chemical expansion

HT-XRD measurements were performed in dry O_2 and wet O_2 (p_{H_2O} = 0.0312 atm) to observe the chemical expansion effect due to hydration. Only a single perovskite ($Pm\bar{3}m$) model was used to evaluate the lattice constant to reflect an average influence from the humidity on the crystal structure. As shown in **Fig 3**, the lattice constants are obviously larger in wet O_2 than in the dry one for the samples doped with Y, In, Gd and Tm. It is because by substituting the tetravalent Zr cations ($Zr_{Zr}^{\times}$) with trivalent dopant cations ($M_{Zr}^{'}$), oxide ion vacancies generates due to charge compensation (eqn (2)), which therefore benefits the hydration reaction (eqn (1)).

$$2Zr_{Zr}^{\times} + M_2O_3 + O_O^{\times} \rightarrow 2M_{Zr}^{'} + 2ZrO_2 + V_O^{\bullet\bullet} \tag{2}$$

It should be noted that the lattice constants in dry O_2 in the low temperature range (30 – 400 ^oC) exhibit a positive deviation from the predicted tendency by extrapolating the data from the high temperature range (700 – 1000 ^oC), shown as dashed line in **Fig 3**. Such phenomenon indicates that the samples were slightly hydrated at the low temperature range, since it is quite difficult to entirely remove water vapor to produce an absolutely dry environment.

In contrary, as shown in **Fig 4**, the lattice constants of the Pr and Tb-doped samples are very close in the wet and dry atmospheres. Such phenomenon is analogous to that of the undoped $BaZrO_3$. Pr and Tb are therefore highly possible to be mainly tetravalent in O_2 atmosphere.

A summarization of the lattice constants at 300 ^oC in dry and wet O_2 atmosphere is shown in **Fig 5**. The chemical expansion effect is quantitatively evaluated based on the *change ratio of lattice constant* defined as eqn (3), in which $a_{\mathrm{wet}\ O_2}$ and $a_{\mathrm{dry}\ O_2}$ are the lattice constants in wet and dry O_2, respectively. In **Fig 5**, tetravalent radii were adopted for Zr (the undoped $BaZrO_3$), Tb, Pr, and also Dy (Dy is mainly tetravalent in $BaZrO_3$ in oxygen atmosphere [10, 23]), whereas trivalent radii were adopted for the other dopants. [24, 25] For the dopants with the radius not larger than that of Ho(III), the lattice constants for both the hydrated and dehydrated phases tends to increase with the increasing dopant radius. However, when trivalent Gd, Eu and Sm, which are larger than Ho, are doped, the lattice constant decreases with the increasing dopant radius. It is also interesting that the change ratio of lattice constant is obviously higher (> 0.37 %) for the samples doped with Yb, Tm, Er, Y and Ho, indicating a stronger effect of chemical expansion due to water incorporation.

$$\textit{change ratio of lattice constant} = \frac{a_{\mathrm{wet\ O_2}} - a_{\mathrm{dry\ O_2}}}{a_{\mathrm{dry\ O_2}}} \times 100\ \% \tag{3}$$

3.2 Proton concentration

Fig 6 shows the proton concentration per unit cell plotted against the change ratio of lattice constant for the samples doped with trivalent dopants. Besides Sc, quite good correlation is shown between the proton concentration and the change ratio of lattice constant. The proton concentrations are small for the In, Sm , Gd and Eu-doped samples, whose lattice volumes only change slightly due to hydration. For the samples doped with Er, Ho, Tm, Y and Yb, both relatively large change ratio of lattice constant and high proton concentration are confirmed. It is quite reasonable that the proton concentration is a very important factor, but probably not the only one, influencing the chemical expansion effect. However, the sample doped with Sc behaves in a different way. Although its proton concentration is comparable with those of the samples doped with Er, Ho and Yb, its change ratio of lattice volume is obviously smaller.

3.3 Site occupancy of dopants in $BaZrO_3$

Profiles of the 031 diffraction peaks of the samples doped with In, Pr, Gd, Tb, Ho, Er, Tm and Yb are shown in **Fig 7** using circle symbols. The 031 peaks of the In, Pr and Tb-doped $BaZrO_3$ exhibit quite good symmetry. In contrary, the peaks belonging to the samples doped with Gd, Ho, Er, Tm and Yb is obviously asymmetric, which is due to a partial hydration during quench in the ambient atmosphere after sintering at 1600 ^{o}C, similar to the phenomenon of the system doped with Y, Sm and Eu [9, 10].

In order to determine the site occupancy of the dopants, Rietveld refinement was performed. To fit the diffraction patterns of the Gd, Ho, Er, Tm and Yb-doped samples, two perovskite phases ($Pm\overline{3}m$) were used to simulate the hydrated and dehydrated phases, whose whole compositions were treated to be the same as the value determined by ICP-AES (**Table 1**). Since the diffraction peaks exhibit good symmetry for the samples doped with In, Pr and Tb, only one perovskite phase ($Pm\overline{3}m$) was used. For the samples doped with Pr, Gd, Tb, Ho, Er, Tm and Yb, which have slight Ba-deficiency (0.02 - 0.04) in composition, the dopants are determined to partially occupy the Ba-site, as summarized in **Table 2**. But for the In-doped sample, which is also slightly Ba-deficient (0.02) in composition, all the In cations are determined to occupy the Zr-site. By combining the results of our previous study on the site occupancy of Sc, Y, Sm, Eu and Dy in $BaZrO_3$ [9, 10], **Fig 8** gives a summarization of the content of the dopants in the Ba-site. It is interesting to see that in a nearly stoichiometric system with slight Ba-deficiency, the lanthanide elements (Pr, Nd, Sm, Eu, Gd, Tb, Dy, Ho, Er, Tm and Yb) partition over the Ba and Zr-sites, whereas the non-lanthanide elements (Sc, Y and In) only occupy the Zr-site.

3.4 Conductivity of doped $BaZrO_3$

The bulk (intra-grain) conductivities are determined by separating the contribution of bulk conduction to the A.C. impedance spectra [5, 15] obtained at relatively low temperature range, since at higher temperature, only the contributions belonging to the grain boundary conduction and electrode reaction are visible (an example on $BaZr_{0.8}Y_{0.2}O_{3-\delta}$ is given in the supplemental information). The bulk conductivities of the samples doped with Sc, Y, In, Pr, Sm, Eu, Gd, Tb, Dy, Ho, Er, Tm and Yb are thereby determined in the available temperature range, and provided in the supplemental information.

To facilitate the comparison, the bulk conductivities at 300 ^{o}C are plotted in **Fig 9**. The radii of tetravalent Tb and Pr cations are used here. In addition, Dy is trivalent in $BaZrO_3$ in hydrogen atmosphere. [23] For the samples doped with the trivalent cations, higher bulk conductivities were obtained in wet H_2, indicating the generation of proton conduction in a humidified environment. It is clear that the samples doped with trivalent Yb, Tm, Er, Y, Ho and Dy exhibit relatively high conductivity. When comparably smaller (Sc and In) or larger dopants (Gd, Eu and Sm) are doped, the conductivity decreases. Such tendency is generally in accordance with our previous study on the system containing 15 mol% dopants, whose conductivity is measured in wet Ar [7]. In addition, the conductivities of the Tb-doped samples changes little between the measurements in dry and wet H_2, suggesting the charge carriers of protons, and therefore concentration of oxide ion vacancies for the hydration reaction (eqn (1)) is quite limited. Tb is therefore highly possible to be tetravalent even in a reducing atmosphere. However, from the results of HT-XRD measurements performed in O_2 atmosphere (**Fig. 4**), Pr is considered to be mainly tetravalent, since no behavior of chemical expansion due to water incorporation was observed, but the conductivity measurements in H_2 clearly indicates that a humid reducing environment results in an increase in the bulk conductivity. It is reported that tetravalent Pr tends to partially turn to trivalent with a decreasing partial pressure of oxygen in atmosphere. [27] For charge compensation, the concentration of oxide ion vacancies increases, which thereby benefits the proton conduction.

The bulk conductivity was plotted against the proton concentration and the change ratio of lattice constant, respectively, in **Fig. 10**. In most cases, the conductivity seems to have an almost linear relationship with the proton concentration. But as shown in **Fig. 10(a)**, the sample doped with Sc behaves quite differently; that although it has an obviously high proton concentration, its conductivity is very small. However, a quite clear tendency can be seen in **Fig. 10(b)** that the bulk conductivity generally increases with the increasing change ratio of lattice constant due to water incorporation.

3.5 Activation energy and pre-exponential factor

Activation energy (E_a) and pre-exponential term (A) of bulk conduction were evaluated over the temperature range from 100 to 250 ^oC, based on eqn (4), where σ_{bulk} is bulk conductivity, T is temperature, and k_b is Boltzmann's constant. As shown in **Fig. 11**, for the samples doped with trivalent Yb, Tm, Er, Y and Ho, which have the radii between 0.868 Å (Yb(III)) [21] and 0.901 Å (Ho(III)) [21], low activation energy between 0.40 and 0.49 eV (detailed value is given in the supplemental information) were obtained, which are typical value for proton conduction. And the lowest activation energy was determined to be 0.40 eV for $BaZr_{0.8}Tm_{0.2}O_{3-\delta}$ in wet H_2. By doping smaller cations of Sc and In, the activation energy are increased over 0.5 eV in both the wet atmospheres of O_2 and H_2. When larger cations of Gd, Eu and Sm are doped, the activation energy increased monotonically with the increasing dopant radius. In addition, the pre-exponential term shows a tendency to increase with the increasing dopant radius.

$$\sigma_{\mathrm{bulk}} T = A\exp\left(\frac{-E_a}{k_{\mathrm{b}} T}\right) \tag{4}$$

4. Discussion

In a nearly stoichiometric sample containing slight Ba-deficiency, Sc, In and Y are determined to only occupy the Zr-site, whereas the lanthanide elements occupy both the Ba and Zr-sites. Such difference in site occupation seems to be a special property for the lanthanide elements. From the view point of defect chemistry, replacing the divalent Ba cations by the trivalent dopant cations consumes the oxide ion vacancies necessary for the hydration reaction, and is regarded as a considerable reason for the lowered conductivity when Ba-deficiency [12] or a large dopant (like Gd) [7] was introduced. However, we found that the amount of lanthanide elements at the Ba-site is quite limited. Even for the samples doped with Er and Tm, whose amounts at the Ba-site were determined to be 0.014 and 0.011, respectively, their conductivities are comparable with or even high than that of the Y-doped one. The Ba-site occupation of the trivalent dopants might decrease the conductivity, but in the nearly stoichiometric sample containing slight Ba-deficiency, we consider that such negative influence is quite small, and is not the major reason restricting the conductivity.

In most cases, the proton concentration, conductivity, and degree of lattice expansion due to the chemical expansion effect behave in a generally related way. That is, the sample which exhibits high proton conductivity also has relatively high proton concentration and strong chemical expansion effect. However, the Sc-doped sample behaves in an obviously different way; that is, although the proton concentration is obviously high, the conductivity and lattice expansion is small. Therefore, it is quite clear that the proton concentration is not the only factor influencing the proton concentration, the way for proton trapping is no doubt another important factor should be taken into account. [8, 28] It is highly possible that the protons are trapped in a different way (relatively to the case in Y-doped $BaZrO_3$ [8]) in the Sc-doped system, and a further investigation is expected.

Y is regarded to be a good dopant for $BaZrO_3$ to impart high proton conductivity. Dy also exhibits high proton conductivity in wet H_2, but it turns to be tetravalent in O_2 with a dramatic drop in proton conductivity, which restricts its application as an electrolyte in fuel cells. [5, 23] In this work, we found that by introducing the same amount of 20 mol% of the dopants into $BaZrO_3$, Yb and Er imparted comparably high proton conductivities. But by doping Ho and Tm, even higher proton conductivity generated in $BaZrO_3$ (**Fig 9**). If only concerning the conductivity, Ho and Tm are better dopants than Y. However, since Tm is much more expensive than Y and Ho, the latter two are more practically appropriate dopants for proton conductive $BaZrO_3$.

5. Conclusions

In this work, various dopants were doped into $BaZrO_3$, and the conductivities were measured. The samples doped with Tm and Ho have even higher proton conductivity than that of the Y-doped one. A systematic investigation was therefore performed on the dopant site occupancy, the dependence of proton concentration and chemical expansion on dopants, in order to reveal the reason of the difference in conductivity by doping different dopants. In nearly stoichiometric samples with slight Ba-deficiency, Sc, Y and In only occupy the Zr-site, whereas the dopants belonging to the lanthanide group occupy both the Ba and Zr-sites, but their amount in the Ba-site is quite limited to influence the conductivity significantly. In addition, the samples possessing high proton concentrations also exhibit high conductivities in most cases. But the Sc-doped sample behaves in a different way. It has a high proton concentration but a low conductivity. The lattice volume change due to chemical expansion also behaves in a similar way. The change in lattice volume of the Sc-doped $BaZrO_3$ is comparably small, but the samples doped with Yb, Tm, Er, Y and Ho show large lattice expansion, suggesting that for the proton conductive acceptor-doped $BaZrO_3$, the proton conductivity and lattice change due to chemical expansion behaves in a correlated way.

References

1 W. Grover Coors, *J. Power Sources*, 2003, **118**, 150.

2 Y. Okumura, Y. Nose, J. Katayama and T. Uda, *J. Electrochem. Soc.*, 2011, **158**, B1067.

3 Y. Yamazaki, R. Hernandez-Sanchez and S.M. Haile, *Chem. Mater.*, 2009, **21**, 2755.

4 D. Pergolesi, E. Fabbri, A. D'Epifanio, E.D. Bartolomeo, A. Tebano, S. Sanna, S. Licoccia, G. Balestrino and E. Traversa, *Nat. Mater.*, 2010, **9**, 846.

5 D. Han, Y. Nose, K. Shinoda and T. Uda, *Solid State Ionics*, 2012, **213**, 2.

6 R.C.T. Slade, S.D. Flint and N. Singh, *Solid State Ionics*, 1995, **82**, 135.

7 S. Imashuku, T. Uda, Y. Nose, G. Taniguchi, Y. Ito and Y. Awakura, *J. Electrochem. Soc.*, 2009, **156**, B1.

8 Y. Yamazaki, F. Blanc, Y. Okuyama, L. Buannic, J.C. Lucio-Vega, C.P. Grey and S.M. Haile, *Nature Mater.*, 2013, **12**, 647.

9 D. Han, K. Kishida, K. Shinoda, H. Inui and T. Uda, *J. Mater. Chem. A*, 2013, **1**, 3027.

10 D. Han, K. Shinoda and T. Uda, *J. Am. Ceram. Soc.*, 2014, **97**, 643.

11 A.K. Azad, C. Savaniu, S. Tao, S. Duval, P. Holtappels, R.M. Ibberson and J.T.S. Irvine, *J. Mater. Chem*. 2008, **18**, 3414.

12 Y. Yamazaki, R. Hernandez-Sanchez and S.M. Haile, *J. Mater. Chem.*, 2010, **20**, 8158.

13 T. Norby, M. Widerøe, R. Glöckner and Y. Larring, *Dalton Trans.*, 2004, **19**, 3012.

14 J. Wu, R.A. Davies, M.S. Islam and S.M. Haile, *Chem. Mater.*, 2005, **17**, 846.

15 D. Han, K. Kishida, H. Inui and T. Uda, *RSC Adv.*, 2014, **4**, 31589.

16 S. Yamaguchi and N. Yamada, *Solid State Ionics*, 2003, **162**, 23.

17 C. Hiraiwa, D. Han, A. Kuramitsu, A. Kuwabara, H. Takeuchi, M. Majima and T. Uda, *J. Am. Ceram. Soc.*, 2013, **96**, 879.

18 D. Han, M. Majima and T. Uda, *J. Solid State Chem.*, 2013, **205**, 122.

19 D. Han, K. Kojima, M. Majima and T. Uda, *J. Electrochem. Soc.*, 2014, **161**, F977.

20 A.K.E. Andersson, S.M. Selbach, C.S. Knee and T. Grande, *J. Am. Ceram. Soc.*, 2014, **97**, 2654.

21 D. Han, Y. Okumura, Y. Nose and T. Uda, *Solid State Ionics*, 2010, 181, 1601.

22 D. Han, K. Shinoda, S. Tsukimoto, H. Takeuchi, C. Hiraiwa, M. Majima and T. Uda, *J. Mater. Chem. A*, 2014, **2**, 12552.

23 D. Han, T. Uda, Y. Nose, T. Okajima, H. Murata, I. Tanaka and K. Shinoda, *Adv. Mater.*, 2012, **24**, 2051.

24 R.D. Shannon, *Acta Crystallogr. Sect. A*, 1976, **32**, 751.

25 O. Knop and J.S. Carlow, *Can. J. Chem.*, 1974, **52**, 2175.

26 M.A. Thundathil, C.Y. Jones, G.J. Snyder and S.M. Haile, *Chem. Mater.*, 2005, **17**, 5146.

27 C.Y Jones, J. Wu, L. Li and S.M. Haile, *J. Appl. Phys.*, 2005, **97**, 114908.

28 F. Blanc, L. Sperrin, D. Lee, R. Dervisoğlu, Y. Yamazaki, S.M. Haile, G. De Paëpe and C.P. Grey, *J. Phy. Chem. Lett.*, 2014, **5**, 2431.

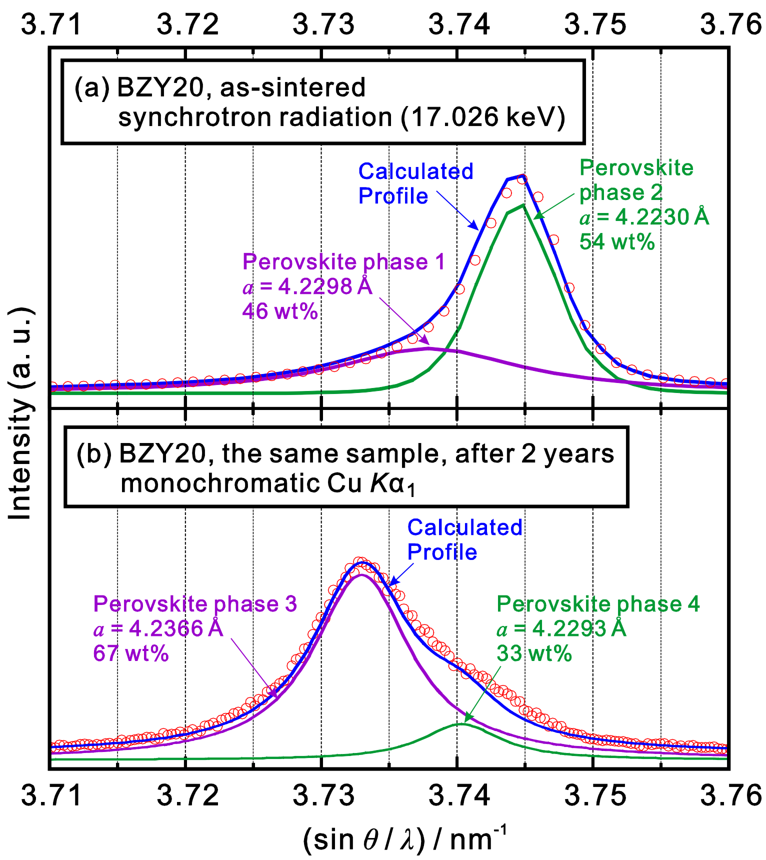

Fig. 1 031 diffraction peaks of the $BaZr_{0.8}Y_{0.2}O_{3-\delta}$ (BZY20) samples (a) as-sintered at 1600 °C and subsequently quenched in ambient atmosphere [11], and (b) after keeping for 2 years in a dessicator, in which the partial pressure of water vapor was controlled to be around 0.003 atm. As reported in our previous work [11], the XRD pattern of the as-sintered sample was collected by synchrotron radiation (17.026 eV), and was simulated by Rietveld refinement using a model containing of two perovskite phases, which had lattice constants of 4.2230 (hydrated phase, 46wt%) and 4.2298 Å (dehydrated phase, 54 wt%), respectively. [11] The XRD pattern of the same sample was collected again by Cu *K*α1 monochromatic X-ray source. Two perovskite phases were simulated to coexist, and their lattice constants were 4.2293 (67 wt%) and 4.2366 Å (34 wt%), respectively.

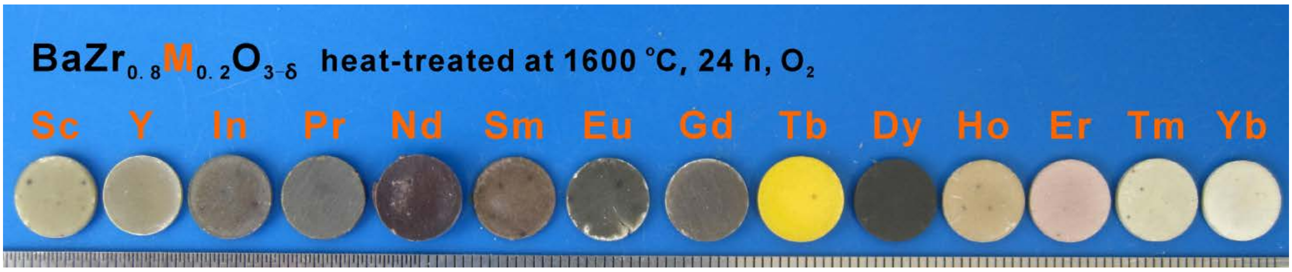

Fig. 2 Photograph of the appearance of the pellets of $BaZr_{0.8}M_{0.2}O_{3-\delta}$ (M = Sc, Y, In, Pr, Nd, Sm, Eu, Gd, Tb, Dy, Ho, Er, Tm, Yb, and In). All the samples were finally heat-treated at 1600 °C in O_2 for 24 h for sintering.

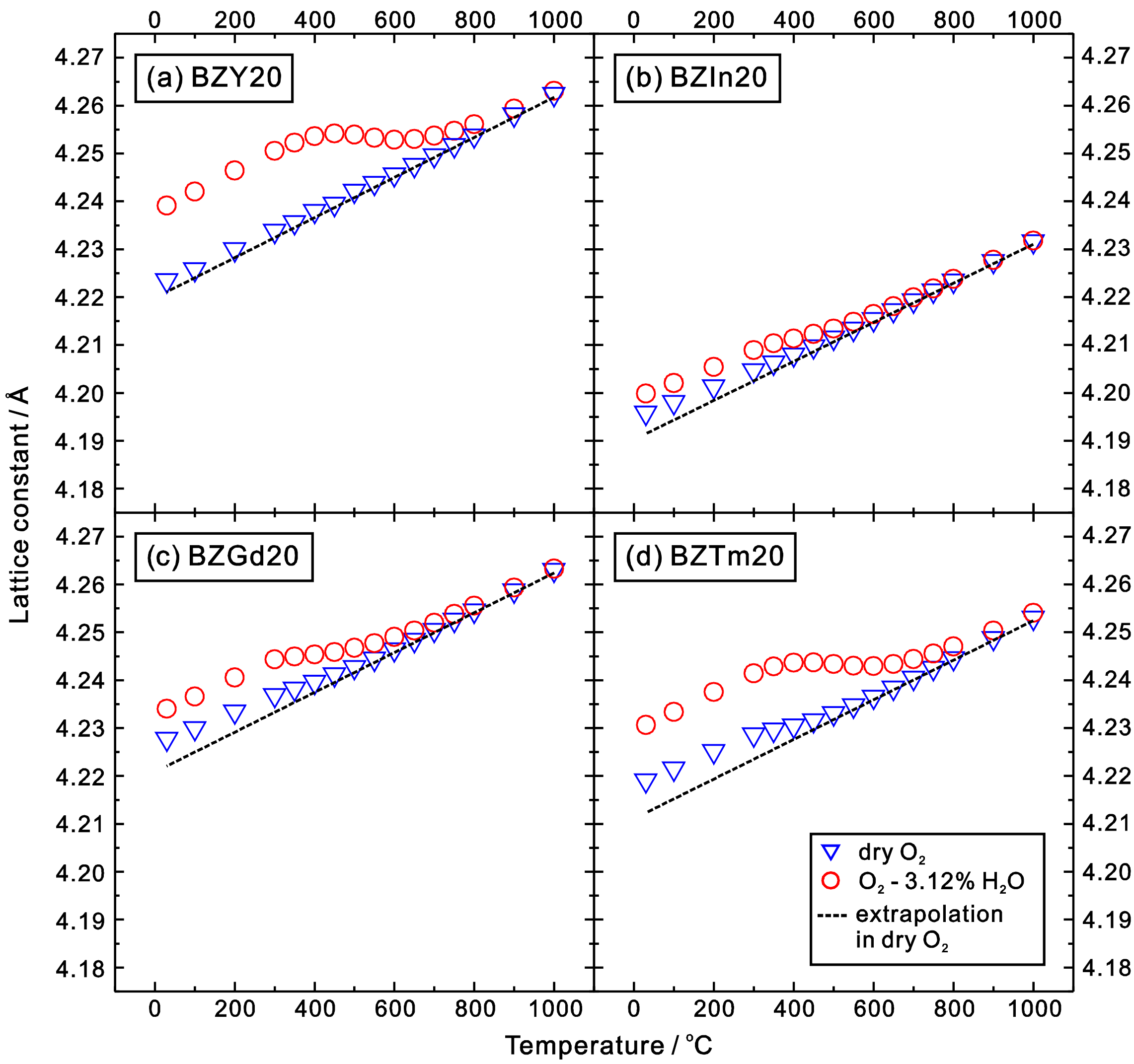

Fig. 3 Variation of lattice constants of (a) $BaZr_{0.8}Y_{0.2}O_{3-\delta}$ (BZY20), (b) $BaZr_{0.8}In_{0.2}O_{3-\delta}$ (BZIn20), (c) $BaZr_{0.8}Gd_{0.2}O_{3-\delta}$ (BZGd20), and (d) $BaZr_{0.8}Tm_{0.2}O_{3-\delta}$ (BZTm20) in dry O_2 and wet O_2 (p_{H_2O} = 0.0312 atm) with temperature. All the samples were finally heat-treatment at 1600 °C in O_2 for 24 h for sintering. The dashed line indicates the extrapolation using the data obtained in the temperature range of 700 to 1000 °C in dry O_2. See **Fig S1** for the case of other dopants (Sc, Sm, Eu, Dy, Ho, Er and Yb). The same phenomenon was observed.

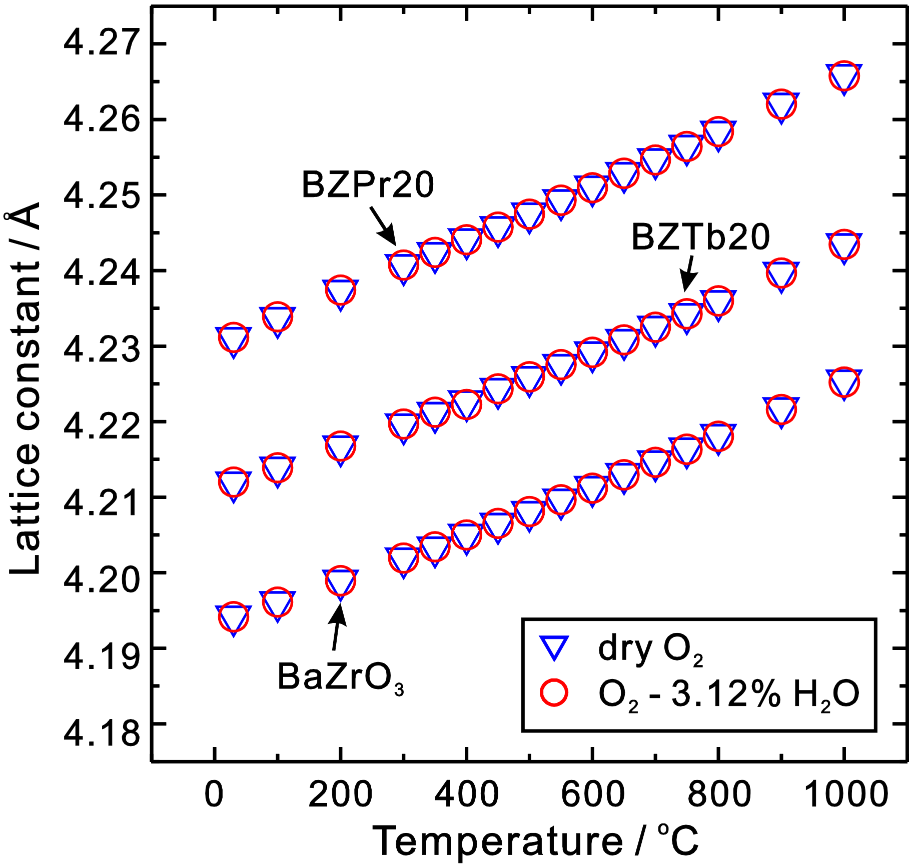

Fig. 4 Variation of lattice constants of undoped $BaZrO_3$, $BaZr_{0.8}Pr_{0.2}O_{3-\delta}$ (BZPr20) and $BaZr_{0.8}Tb_{0.2}O_{3-\delta}$ (BZTb20) in dry O_2 and wet O_2 ($p_{H_2O} = 0.0312$ atm) with temperature. All the samples were finally heat-treatment at 1600 °C in O_2 for 24 h for sintering

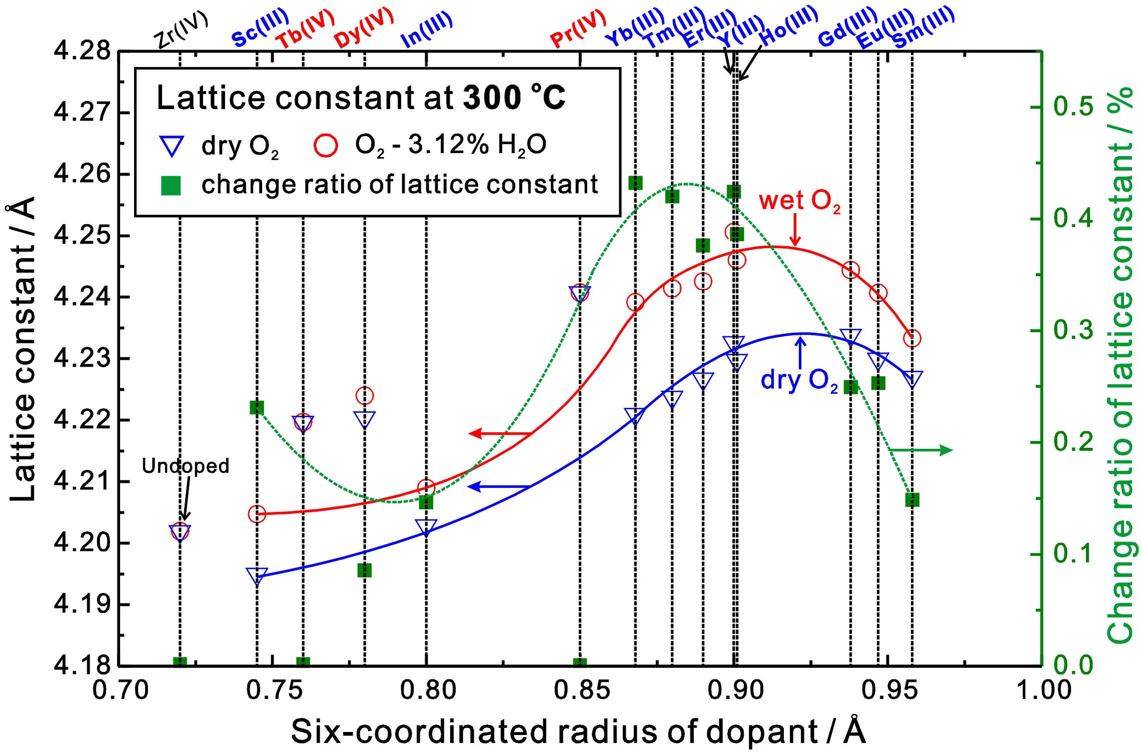

Fig. 5 Lattice constant of the samples of undoped $BaZrO_3$ and those doped with rare earth elements and In at 300 °C, determined from HT-XRD measurements. The lattice constants in dry and wet O_2 atmosphere were marked using open triangles and circles, respectively. Change ratio of the lattice constant was marked using solid square symbols. All the samples were sintered at 1600 °C in O_2 for 24 h before the HT-XRD measurements. In dry O_2, the values determined by extrapolation were used. Solid and dash lines are used to highlight the tendency of variation with the increasing dopant radius for the lattice constants of the samples doped with trivalent cations (Sc, In, Yb, Tm, Er, Y, Ho, Gd, Eu and Sm) and their change ratio. See **Fig. S2** for the cases at 30 and 600 °C.

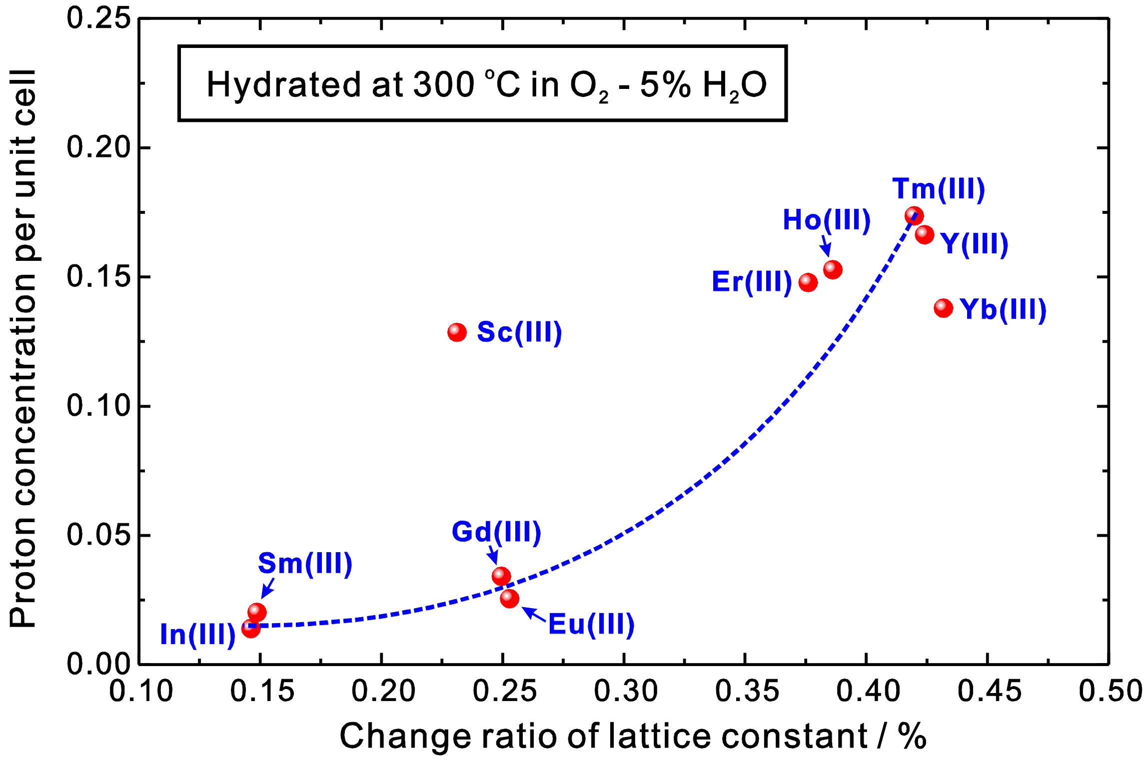

Fig. 6 Proton concentration of $Ba(Zr_{0.8}M_{0.2})O_{3-\delta}$ (M = Sc, Y, In, Sm, Eu, Gd, Ho, Er, Tm, Yb) at 300 °C plotted against the change ratio of lattice constant. The change ratio of lattice constant was determined by HT-XRD measurement performed in dry and wet ($p_{H_2O} = 0.0312$ atm) O_2. The proton concentration was determined by Karl-Fischer titration method to measure the water content in the samples hydrated at 300 °C in O_2 – 5% H_2O. The data of samples doped with Sc, Y, Sm and Eu were cited from our previous work [5].

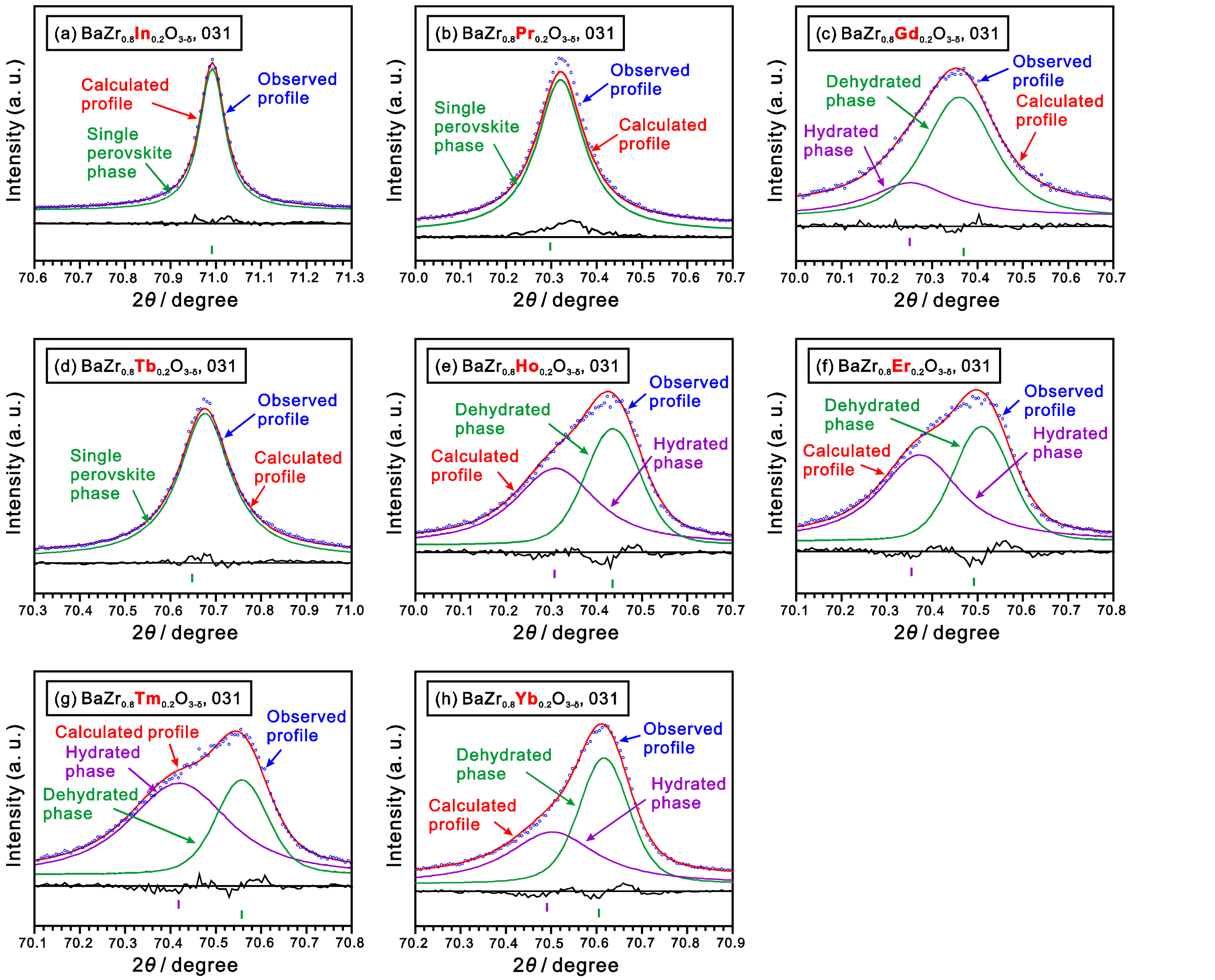

Fig. 7 Rietveld refinement of the 031 diffraction peaks of $BaZr_{0.8}M_{0.2}O_{3-\delta}$ (M = In, Pr, Gd, Tb, Ho, Er, Tm and Yb). The diffraction patterns were collected using a Cu $K\alpha_1$ monochromatic X-ray source. Before the XRD measurements, all the samples were sintered at 1600 °C in O_2 for 24 h, and finally quenched in ambient atmosphere. A cubic perovskite ($Pm\bar{3}m$) structure was used to simulate all the phases. Observed profile (blue circle), calculated profile (red line), difference (black line at bottem), and Bragg peaks of candidate phases (vertical lines) are shown.

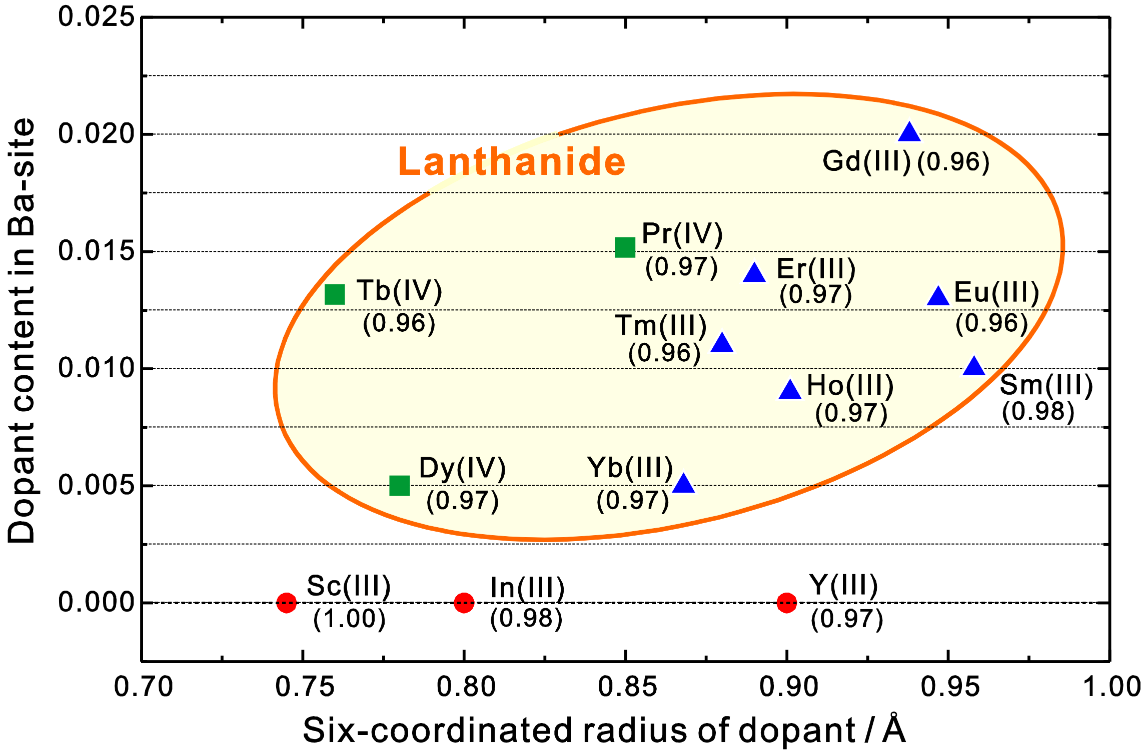

Fig. 8 Dopant content in Ba-site determined by Rietveld refinement. The Ba-deficiency for all the sample was no more than 0.04. The content of Sc, Y, Sm, Eu and Dy in the Ba-site was cited from our previous works [11, 12]. The Ba contents of the samples were given in brackets. Although the radius of tetravalent Pr cations is used here, there exists the possibility that Pr in the A-site of perovskite structure is trivalent. [26]

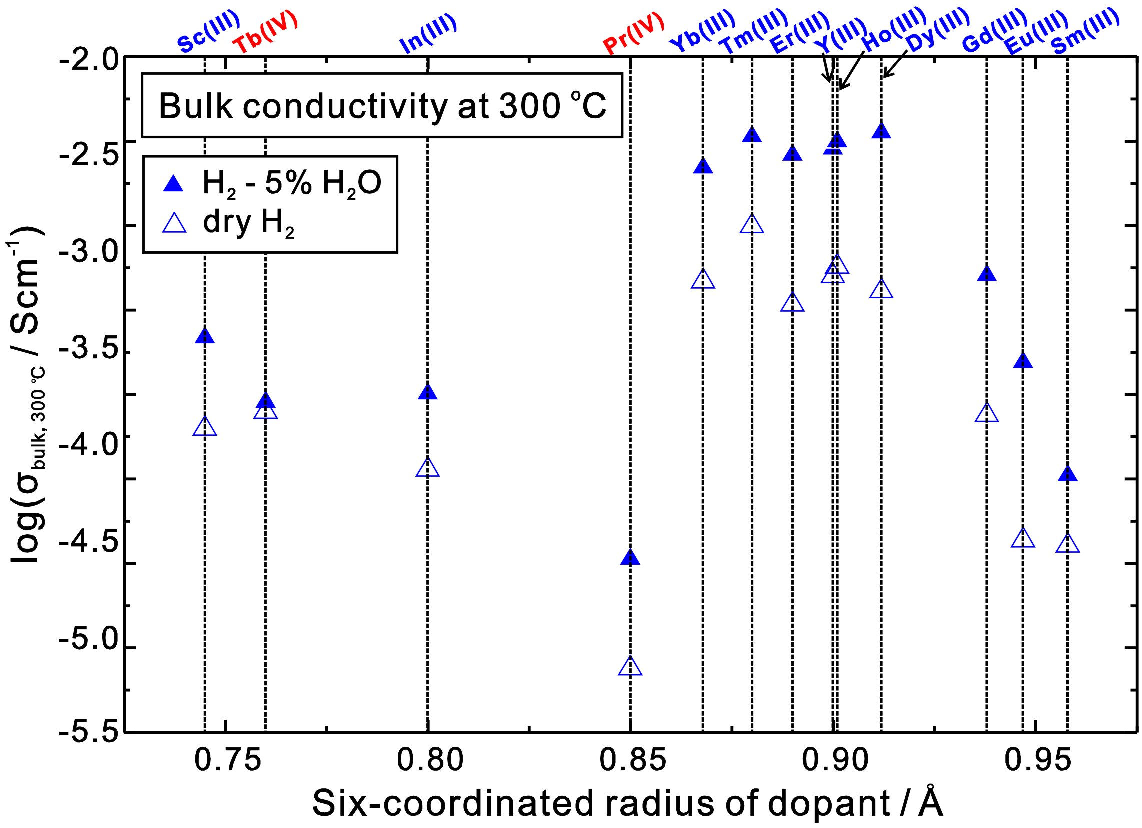

Fig. 9 Bulk conductivity of acceptor-doped $BaZrO_3$ at 300 °C in dry and wet atmospheres of H_2. Water partial pressure was kept at 0.05 atm. All the samples were sintered at 1600 °C in O_2 for 24 h before the conductivity measurements.

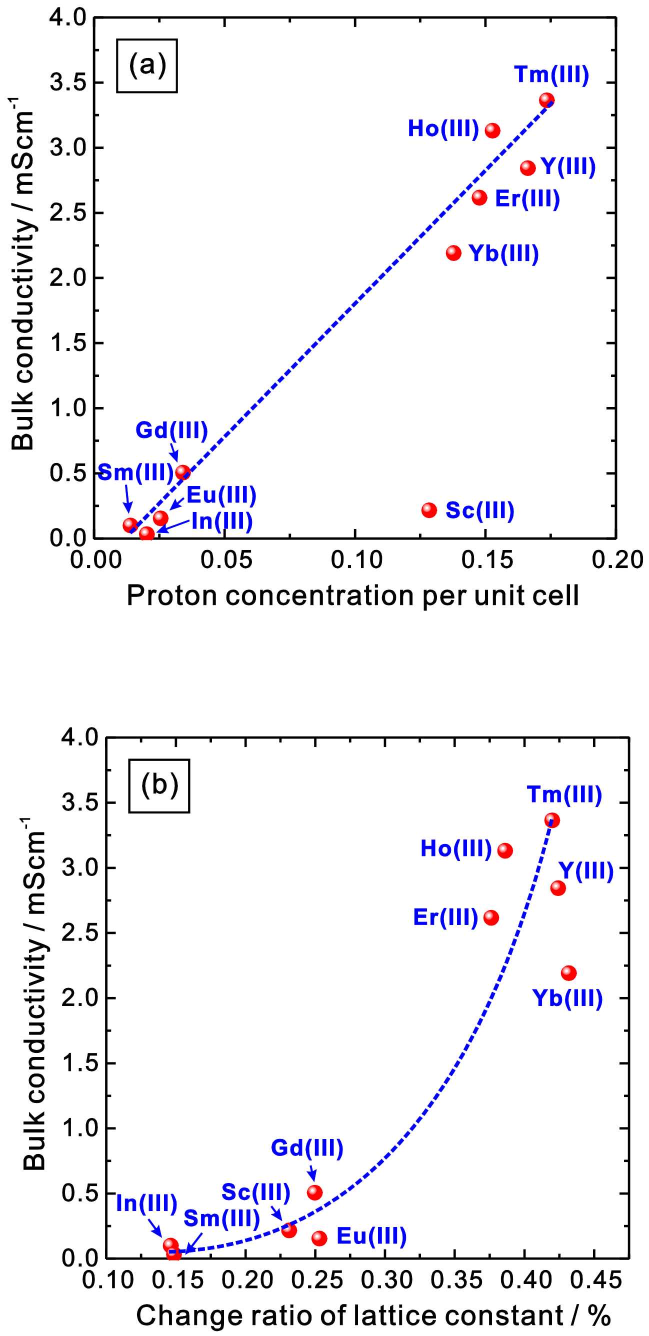

Fig. 10 Bulk conductivity of $Ba(Zr_{0.8}M_{0.2})O_{3-\delta}$ (M = Sc, Y, In, Sm, Eu, Gd, Ho, Er, Tm, Yb) at 300 °C plotted against (a) the change ratio of lattice constant, and (b) the change ratio of lattice constant. The proton conductivity was measured in H_2 – 5% H_2O atmosphere. The change ratio of lattice constant was determined by HT-XRD measurement performed in dry and wet (p_{H_2O} = 0.0312 atm) O_2.

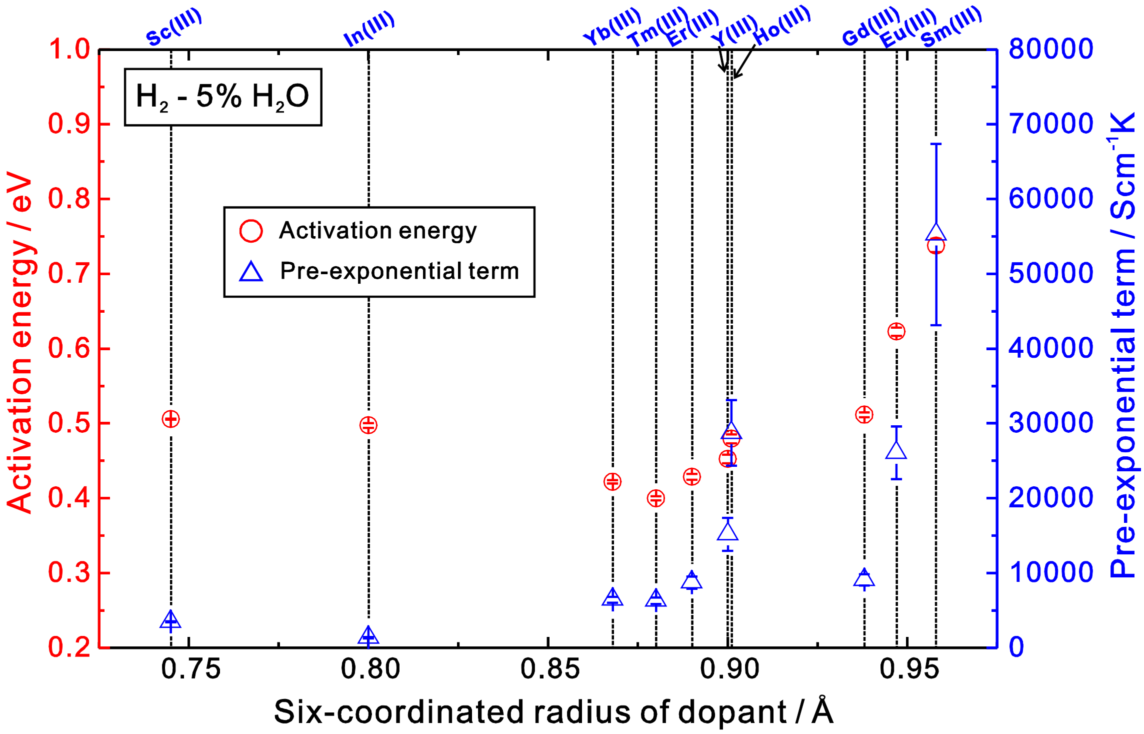

Fig. 11 Activation energy (red open circle) and pre-exponential term (blue open triangle) of the bulk conduction in $BaZrO_3$ doped with trivalent rare earth elements (Sc, Y, Sm, Eu, Gd, Ho, Er, Tm, Yb) in H_2 – 5% H_2O.

Table 1 Actual composition of $BaZr_{0.8}M_{0.2}O_{3-\delta}$ (M = In, Pr, Gd, Tb, Ho, Er, Tm and Yb) determined by ICP-AES.

Nominal composition	Actual composition by ICP-AES
$BaZr_{0.8}In_{0.2}O_{3-\delta}$	$Ba_{0.98}Zr_{0.83}In_{0.17}O_{3-\delta}$
$BaZr_{0.8}Pr_{0.2}O_{3-\delta}$	$Ba_{0.97}Zr_{0.82}Pr_{0.18}O_{3-\delta}$
$BaZr_{0.8}Gd_{0.2}O_{3-\delta}$	$Ba_{0.96}Zr_{0.80}Gd_{0.20}O_{3-\delta}$
$BaZr_{0.8}Tb_{0.2}O_{3-\delta}$	$Ba_{0.96}Zr_{0.82}Tb_{0.18}O_{3-\delta}$
$BaZr_{0.8}Ho_{0.2}O_{3-\delta}$	$Ba_{0.97}Zr_{0.81}Ho_{0.19}O_{3-\delta}$
$BaZr_{0.8}Er_{0.2}O_{3-\delta}$	$Ba_{0.97}Zr_{0.81}Er_{0.19}O_{3-\delta}$
$BaZr_{0.8}Tm_{0.2}O_{3-\delta}$	$Ba_{0.96}Zr_{0.81}Tm_{0.19}O_{3-\delta}$
$BaZr_{0.8}Yb_{0.2}O_{3-\delta}$	$Ba_{0.97}Zr_{0.81}Yb_{0.19}O_{3-\delta}$

Table 2 Rietveld refinement results of the diffraction patterns of $BaZr_{0.8}M_{0.2}O_{3-\delta}$ (M = In, Pr, Gd, Tb, Ho, Er, Tm and Yb) collected with Cu $K\alpha1$ monochromatic X-ray source. The structures of all the phases were assigned to be cubic ($Pm\bar{3}m$). All the samples were sintered at 1600 °C in O_2 for 24 h, and finally quenched in ambient atmosphere.

Nominal sample composition	R_{wp} / %	χ^2	Phase (composition)	Lattice constant / Å	Fraction / wt%	Site occupancy				Equivalent isotropic temperature factor / Å^2	
						A-site		B-site			
						Ba	M	Zr	M	A-site	B-site
$BaZr_{0.8}In_{0.2}O_{3-\delta}$	6.11	1.12	$Ba_{0.98}Zr_{0.83}In_{0.17}O_{3-\delta}$	4.1965(2)	100.00	0.980(1)	0.000(1)	0.830(1)	0.170(1)	0.20(2)	0.20(2)
$BaZr_{0.8}Pr_{0.2}O_{3-\delta}$	9.53	2.12	$Ba_{0.97}Zr_{0.82}Pr_{0.18}O_{3-\delta}$	4.2312(3)	100.00	0.985(2)	0.015(2)	0.802(2)	0.198(2)	0.71(2)	0.20(2)
$BaZr_{0.8}Gd_{0.2}O_{3-\delta}$	5.74	1.08	Dehydrated phase ($Ba_{0.96}Zr_{0.80}Gd_{0.20}O_{3-\delta}$)	4.2291(3)	66.99	0.980(1)	0.020(1)	0.816(1)	0.184(1)	0.80(5)	0.20(6)
			Hydrated phase ($Ba_{0.96}Zr_{0.80}Gd_{0.20}O_{3-\delta}$)	4.2348(3)	33.01	0.980(1)	0.020(1)	0.816(1)	0.184(1)	0.80(2)	0.32(2)
$BaZr_{0.8}Tb_{0.2}O_{3-\delta}$	6.44	1.18	$Ba_{0.96}Zr_{0.82}Tb_{0.18}O_{3-\delta}$	4.2129(2)	100.00	0.972(2)	0.013(2)	0.830(2)	0.170(2)	0.40(3)	0.20(3)
$BaZr_{0.8}Ho_{0.2}O_{3-\delta}$	7.21	1.16	Dehydrated phase ($Ba_{0.97}Zr_{0.81}Ho_{0.19}O_{3-\delta}$)	4.2250(2)	43.46	0.979(2)	0.009(2)	0.817(1)	0.183(1)	0.80(5)	0.25(5)
			Hydrated phase ($Ba_{0.97}Zr_{0.81}Ho_{0.19}O_{3-\delta}$)	4.2316(2)	56.54	0.979(2)	0.009(2)	0.817(1)	0.183(1)	0.80(5)	0.42(5)
$BaZr_{0.8}Er_{0.2}O_{3-\delta}$	7.08	1.18	Dehydrated phase ($Ba_{0.97}Zr_{0.81}Er_{0.19}O_{3-\delta}$)	4.2210(3)	41.32	0.984(2)	0.014(2)	0.821(9)	0.179(9)	0.80(5)	0.20(5)
			Hydrated phase ($Ba_{0.97}Zr_{0.81}Er_{0.19}O_{3-\delta}$)	4.2283(3)	58.68	0.984(2)	0.014(2)	0.821(9)	0.179(9)	0.80(4)	0.31(4)
$BaZr_{0.8}Tm_{0.2}O_{3-\delta}$	7.07	1.13	Dehydrated phase ($Ba_{0.96}Zr_{0.81}Tm_{0.19}O_{3-\delta}$)	4.2177(3)	45.30	0.970(2)	0.011(2)	0.819(1)	0.181(1)	0.49(6)	0.20(6)
			Hydrated phase ($Ba_{0.96}Zr_{0.81}Tm_{0.19}O_{3-\delta}$)	4.2249(2)	54.70	0.970(2)	0.011(2)	0.819(1)	0.181(1)	0.800(4)	0.39(4)
$BaZr_{0.8}Yb_{0.2}O_{3-\delta}$	7.52	1.58	Dehydrated phase ($Ba_{0.97}Zr_{0.81}Yb_{0.19}O_{3-\delta}$)	4.2150(2)	49.57	0.975(2)	0.005(2)	0.814(2)	0.186(2)	0.50(4)	0.20(4)
			Hydrated phase ($Ba_{0.97}Zr_{0.81}Yb_{0.19}O_{3-\delta}$)	4.2206(2)	50.43	0.975(2)	0.005(2)	0.814(2)	0.186(2)	0.80(5)	0.80(5)